PAPER

Check for updates

Antibacterial surface based on hierarchical polyurethane acrylate/zinc oxide structures

Sruthi Venugopal Oopath,[a] Akesh Babu Kakarla,[b] Ing Kong,[b] Thanh Tien Nguyen,[c] Vi Khanh Truong [ID]*[c] and Avinash Baji [ID]*[a]

In this study, we fabricated hierarchical structures on the surface of polyurethane acrylate (PUA) film and demonstrated that the film displays antibacterial properties. PUA resin was coated on a commercial porous anodized aluminum oxide (AAO) template and was UV-cured using nanoimprint lithography. This led to the formation of 150 nm diameter pillars on the surface of PUA film. Following this, zinc oxide structures were grown on the surface of this imprinted PUA sample using a hydrothermal method. The scanning electron microcopy and Fourier transform infrared spectroscopy results confirmed the presence of ZnO on the surface of the PUA film. The antibacterial behavior of the fabricated sample was demonstrated against *Staphylococcus aureus* (*S. aureus*) and *Pseudomonas aeruginosa* (*P. aeruginosa*) as model bacteria. The results show that PUA film with 150 nm diameter pillars had moderate antibacterial properties against both *S. aureus* and *P. aeruginosa*. The presence of zinc oxide (ZnO) structures improved the film's antibacterial property to ~100% against *P. aeruginosa*. However, the presence of ZnO structures on PUA film is shown to have no effect against *S. aureus*. This can be attributed to the shape and size of the fabricated ZnO structures.

1. Introduction

Antibacterial materials have gained a significant amount of interest in recent years with an aim to inhibit and prevent the growth and proliferation of bacteria.[1-4] Antibacterial materials play a significant role in combating the spread of bacterial infections and hence have found applications in healthcare, food packing and water treatment.[5-9] A wide variety of strategies and fabrication approaches have been employed in the design of antibacterial materials.[10-13] A typical approach used to produce antibacterial materials is to incorporate antibacterial agents, such as biocides or chemicals into the material.[5] However, the effectiveness of these materials largely depends on the distribution of the antibacterial agents and their interaction with the surrounding environment. One promising approach to produce antibacterial materials involves surface modification and the introduction of textured surfaces.[10] Surface structures play a key role in determining the antibacterial properties of the material, as they influence surface characteristics such as surface energy, roughness, and wettability.[14] Introducing surface textures ensure that the material

can inhibit bacterial attachment and colonization on the surface, as the surface structures directly interact with the bacteria.[5,10,14]

Various types of surface structures, such as micro and nanotextures, as well as hierarchical structures, have been developed and explored for their potential antibacterial applications.[10,11,15] Micro and nanostructures can interact with bacterial cells in various ways. They can physically interact with the bacterial cells, leading to their rupture. They also can create a repulsive charge that inhibits the bacterial cells from adhering.[5,16-19] It is argued that the mechanism of interaction between the surface structures and bacterial cells depend on the size and aspect ratio of the structures, as well as the type of bacteria involved.[5] Achieving precise control over the morphology of surface nano- and microstructures is key to maximizing their antibacterial effectiveness. Techniques such as chemical modification, physical patterning using nanoimprint lithography, electrospinning and surface coating have been used to produce micro and nanoscale structures on polymer films using.[10,17,19-21] Among these techniques, nanoimprint lithography (NIL) has emerged as a powerful technique for fabricating surface structures with precise control over their size, shape, and orientation.[22] This technique involves the transfer of patterns from a template to a substrate using pressure and heat or using pressure and a UV source. It results in highly precise and efficient fabrication of micro and nanoscale structures on the surface of the polymer film. Inorganic metal oxide nanoparticles have also been shown to be antibacterial.[23-27] For example, zinc oxide (ZnO) particles are shown to be

[a] Department of Engineering, La Trobe University, Bundoora 3086, Victoria, Australia. E-mail: a.baji@latrobe.edu.au

[b] Department of Engineering, La Trobe University, Bendigo 3446, Victoria, Australia

[c] Biomedical Nanoengineering Laboratory, College of medicine and Public Health, Flinders University, Bedford Park 5042, South Australia, Australia. E-mail: vikhanh.truong@flinders.edu.au

antibacterial against Gram-positive and Gram-negative bacteria.[28,29] Nanoparticles of ZnO employ a few mechanisms of actions against bacterial cells. They generate reactive oxygen species (ROS), bind to proteins and DNA and cause disturbance of the bacterial DNA amplification.[28] Studies have used ZnO nanoparticles and distributed them in a polymer matrix to impart antibacterial properties to the polymer.[30–32] They show that the presence of ZnO enables the polymer composite to kill and inhibit the growth of bacteria.

In this study, we employed nanoimprint lithography to produce 150 nm diameter pillars on the surface of polyurethane acrylate (PUA) film. Following this, we employed a hydrothermal method to grow secondary zinc oxide (ZnO) nanostructures on the surface of these imprinted PUA film. Subsequently, we demonstrated the antibacterial properties of these structures against Gram-positive *Staphylococcus aureus* and Gram-negative *Pseudomonas aeruginosa*. Our findings indicate that the hierarchical structures demonstrate excellent antibacterial properties against *P. aeruginosa*. However, the presence of ZnO did not improve the antibacterial properties against *S. aureus*. One possible reason could be that the density of ZnO was not adequate to fully eliminate *S. aureus*. In future studies, we plan to adjust the processing parameters to control the aspect ratio and density of ZnO structures with an aim to achieve the most optimal antibacterial properties.

2. Materials and methods

2.1. Materials

Polyurethane-acrylate (PUA, MINS-301RM) precursor was obtained from Minuta Tech. Co. Ltd (Korea). Porous anodized aluminium oxide (AAO) templates with ~150 nm pore size was obtained from Shanghai Shangmu Technology Co., Ltd (Shanghai, China). 1*H*,1*H*,2*H*,2*H*-Perfluorooctyl-trichlorosilane (PTCS), triethylamine, zinc acetate dihydrate, hexamethylenetetramine (HMTA), zinc nitrate hexahydrate, poly(vinyl alcohol) (PVA, with average molecular weight 130 000) were obtained from Sigma-Aldrich (Macquarie Park, NSW, Australia). Dimethylformamide (DMF), acetone, ethanol and isopropanol were obtained from CSA Scientific (Gillman, SA, Australia).

2.2. Preparation of PUA film with hierarchical structures

PUA precursor was spin coated on the surface of a porous AAO template (150 nm pore diameter). AAO template coated with PUA layer was placed between two Teflon films and was transferred to the Compact Imprinting tool (CNI, NIL Technology ApS, Kongens Lyngby, Denmark). A vacuum pressure of 1 bar was applied during the imprinting step to enable the flow of PUA into the pores of AAO template. Following this, the set up was exposed to a UV source for 1 min (50% power) to cure PUA. Cured PUA film was demoulded from the AAO template to reveal 150 nm sized pillars on the surface of PUA. PUA film with 150 nm diameter is called Sample 1.

2.3 Fabrication of ZnO nanostructures

ZnO nanostructures were grown on Sample 1 using a hydrothermal method as reported in literature.[33–35] ZnO structures were grown on Sample 1 by treating it with a ZnO seed solution and a ZnO growth solution. To prepare the seed solution, 1.0975 g of zinc acetate dihydrate (0.1 M) was dissolved in 50 ml of isopropanol solution along with 0.01 g of polyvinyl alcohol at 85 °C for 1 h using a hot-plate stirrer. 0.1 M triethylamine was added dropwise into this solution until it turned from cloudy to clear solution. This reaction was remained at 85 °C for 10 min. Following this, the solution was aged at room temperature for 3 h. Growth solution was prepared by dissolving 1.928 g of hexamethylene tetramine (HMTA) (0.025 M) in 550 ml of deionised (DI) water. 4.09 g of zinc nitrate hexahydrate (0.025 M) was added to this solution and stirred for 24 h using a magnetic stirrer.

Sample 1 was first dipped into the seed solution for 8 min and then rinsed with ethanol. Subsequently, it was heat treated in an oven at 120 °C for 1 h and dried in air for 24 h. This enabled the deposition of a uniform ZnO seed layer on Sample 1. Following this, the sample was dipped in the growth solution. The set up was then placed in a closed glass vial and heated at 95 °C for 8 h. In the final step, the sample was washed with DI water. This PUA sample with 150 nm diameter pillars and ZnO nanostructures is referred to as Sample 2.

2.4 Characterization

Hitachi TM4000 (NewSpec Pty Ltd Australia) tabletop scanning electron microscopy (SEM) was used to examine the surface of both samples. Before the examination, the samples were sputter coated with a thin layer of platinum (18 mA, 60 s) using a sputter coater (Safematic CCU-010 HV sputter coater, Microscopy Solutions Pty Ltd, Australia). Accelerating voltage of 5 kV was used during the SEM visualization.

Energy dispersive spectroscopy (EDS) (Hitachi TM3030 Plus with Brucker EDS, NewSpec Pvt Ltd Australia) was used for the elemental analysis. The samples were coated with a thin layer of carbon using a sputter coater before they were analysed using EDS.

2.5 Fourier transform infrared (FTIR)

Shimadzu spectrometer (IRAffinity – IS) was used to determine the presence of ZnO on the Sample 2. The IR spectra were obtained in the wavenumber range of 3600–700 cm^{-1} in transmittance mode and at the resolution of 4 cm^{-1}.

2.6 Bacterial culture and incubation

The antibacterial properties of the samples were tested against *S. aureus* and *P. aeruginosa*. The tryptone soy broth (TSB) was used to grow these types of bacteria for a period of 18 h with conditions at 37 °C and 200 rpm. The final bacterial suspension was collected and diluted to obtain $OD_{600} = 0.1$ in TSB medium for antibacterial inhibition testing. The antibacterial behaviour of the samples was investigated by testing the surface. Briefly, the samples were cut into squares with dimensions of 1 cm × 1 cm. Next, they were glued to a silicon wafer using a double-sided tape. Subsequently, they were placed in each well of the 24-well plate. 400 μl bacterial suspensions (*S. aureus* and *P. aeruginosa*) of early-log-phase bacterial culture (diluted in TSB, $OD_{600} = 0.1$) were added to the wells containing the samples. The well plate was

incubated for 18 h at 37 °C under static circumstances. After incubation, the samples were gently washed with PBS twice to prepare for confocal laser scanning microscopy. The cells were examined using a confocal laser scanning microscopy (CLSM). The Living/DEAD® BacLightTM Bacterial Viability Kit, L7012 (Molecular ProbesTM, Invitrogen, USA), was used to quantify the percentages of living and dead cells. This kit comprised of fluorescent dye SYTO® 9 and propidium iodide (PI). 10 µl of diluted LIVE/DEAD® BacLight™ dye solutions was placed on surface of Sample 1 and Sample 2, followed by the incubation in the dark for 15 minutes. SYTO® 9 is able to enter all bacterial cells where it binds to nucleic acids and emits a green fluorescent signal. Propidium iodide (PI) has a higher affinity for nucleic acids than SYTO® 9 and enters only severely damaged and dead cells. The wavelengths that are used to excite the luminescence of SYTO® 9 and PI were 485 nm and 488 nm laser respectively. Dual emission filter of CLMS was set up to inspect both live bacterial cells in green (SYTO9, Ex/Em 480/500 nm) and dead bacterial cells in red (PI, Ex/Em 490/635 nm). Three surface images of the sample were randomly selected for use in the analysis of the ratio of viable to dead cells. Zen Black and ImageJ analysis software (Version 9.3.0, Bitplane, Zürich, CHE) were used to investigate the surface photos, and the percentage of green and red pixels with a diameter of around 4–600 nm was counted to establish the antibacterial level.[36]

3. Results and discussion

Certain natural materials such as cicada wings and dragonfly wings, have evolved to display mechano-bactericidal behaviour due to the presence of nanostructures on their wings.[14,37] These surface nanostructures physically interact with bacterial cells, leading to their inactivation or destruction.[15,37] Researchers have also fabricated synthetic antibacterial materials by introducing nanoneedles, nanowhiskers and other nanostructures onto the surface of polymer films.[5,38–40] These synthetic materials with surface nanostructures are shown to display similar mechano-bactericidal behaviour as their biological counterparts. The sharp nanostructures puncture the bacterial cell membranes, causing the leakage of cellular contents and ultimately resulting in the death of bacterial cells.[40–42] In this study, we produced hierarchical structures on the surface of PUA film and demonstrated that these structures enable the PUA to exhibit antibacterial properties.

Initially, PUA prepolymer is coated on the surface of porous AAO template. UV-based nanoimprinting is then used to obtain the negative replica of porous AAO template onto the PUA film, resulting in the formation of structures on the surface of the PUA film as shown in Fig. 1(A). These structures are visible as 150 nm sized pillars on the surface of the PUA film. In the subsequent step, a hydrothermal method is utilized to grow ZnO nanostructures on the imprinted PUA film surface. Fig. 1(B) displays a SEM image of the sample obtained after the growth of ZnO nanostructures. The SEM image reveals the presence of uniformly formed, thorn-like ZnO structures on the entire surface of the sample. The image also shows that these ZnO structures grow on top of the 150 nm diameter pillars, which are still present on the surface.

Following this, energy dispersive X-ray spectroscopy (EDX) was used to determine the elemental composition of PUA film with hierarchical structures. EDX was also used to confirm the formation of ZnO nanostructures on the sample. Fig. 2 shows the EDX spectrum and the elemental map image of PUA film with the hierarchical structures. The elemental map and the spectra clearly reveal the presence of various elements, including zinc and oxygen, with the strong signals corresponding to Zn, O, C and N elements. The peaks observed at 0.3 keV, 0.5 keV and 1.0 keV within the spectra are attributed to the emissions from the K-shell of carbon, K-shell of oxygen, and L-shell of zinc, respectively. The presence of ZnO on the PUA sample is confirmed using EDX. No additional peaks are evident in the spectrum, which indicates the formation of pure ZnO nanostructures on the PUA film via hydrothermal method.

FTIR spectroscopy was utilised to confirm the presence of ZnO. Fig. 3 displays the FTIR spectra of neat PUA film, Sample 1, and Sample 2. The peaks of PUA film and Sample 1 are found to be identical, indicating that the formation of 150 nm diameter
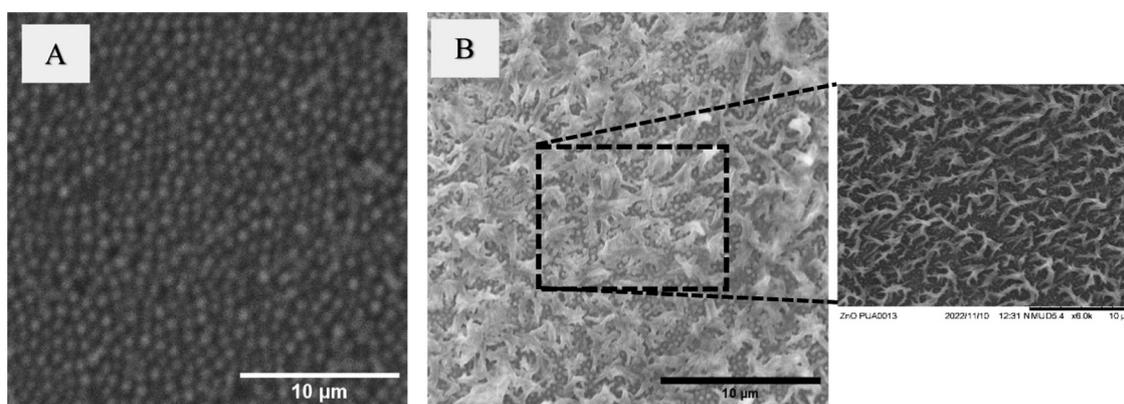

Fig. 1 Scanning electron microscopy (SEM) images of the (A) Sample 1 (PUA film with 150 nm diameter pillars) and (B) Sample 2 (PUA film with hierarchical structures).
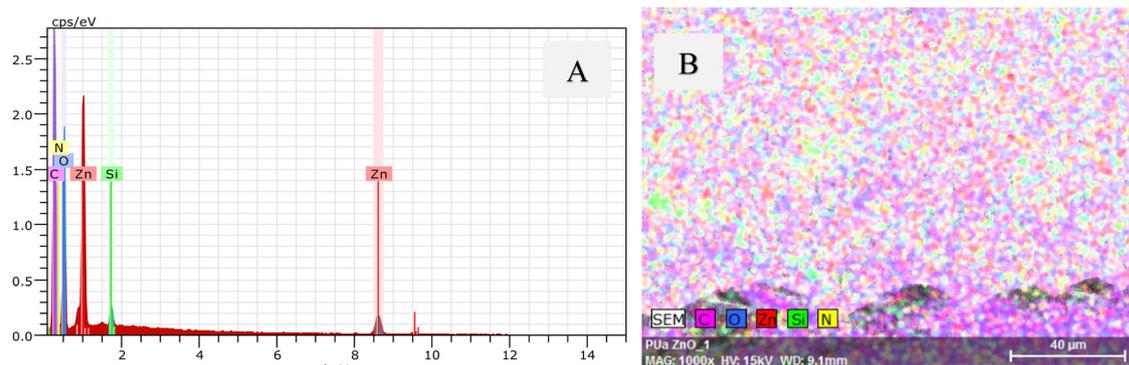
Fig. 2 (A) EDS images of Sample 2 demonstrating the presence of ZnO, and (B) EDX mapping images of Sample 2.

pillars on Sample 1 did not affect its chemical composition. However, FTIR spectra of Sample 2 exhibit additional peaks at 1339 and 1556 cm^{-1}, which can be attributed to the symmetric and asymmetric O–C–O stretching vibration of the carbonate anion respectively. Sample 2 also shows bands at ~1650 and ~1340 cm^{-1} that correspond to the asymmetric and symmetric C=O stretching modes.[43,44] The band at 1040 cm^{-1} can be attributed to the –CH$_2$ vibration. The sharp peak at ~720 cm^{-1} is due to H–O–H bending vibration, attributed to the presence of water during crystallization. Thus, the EDX spectra and the FTIR spectra confirms the formation of ZnO on the surface of the PUA film.

Following this, the antibacterial behaviour of the samples is examined against *P. aeruginosa* and *S. aureus*. For comparison purposes, antibacterial behaviour of control (with no film) is also recorded. It is clear from Fig. 4, that the control sample has mostly live *P. aeruginosa* cells. Compared to the control sample, Sample 1 displays an enhanced antibacterial effect in killing *P. aeruginosa* cells. This can be attributed to the surface energy of the Sample 1. Similar findings are reported by Valiei *et al.*[45] in their study, where they investigated the role of surface wettability on the adhesion of *P. aeruginosa* cells. Surfaces that are

more hydrophilic are shown to be more effective in killing *P. aeruginosa* cells. PUA is an inherently hydrophilic material. It is known that the presence of surface microstructures on a hydrophilic material helps to enhance its hydrophilicity. The increase in hydrophilicity can be attributed to its moderate antibacterial behavior against *P. aeruginosa* cells. On the other hand, almost 100% antibacterial effect is demonstrated by Sample 2 against *P. aeruginosa* cells. Their antibacterial behavior can be attributed to the presence of ZnO. These ZnO structures release zinc ions that have an ability to penetrate the bacterial cell membrane thereby disrupting the functions of the cells and resulting in the death of the cells.[3,41] Gram-negative bacteria such as *P. aeruginosa* have a thin peptidoglycan layer, which provides them with antimicrobial resistance. In addition to this, they also have carboxyl groups present in the membranes, which helps them to generate negative charges on the surface of the cells. The zinc ions produced by ZnO nanoparticles have positive charges. The electrostatic gradient differences across the negatively charged bacterial cells and positively charged zinc generates the electrostatic force, which plays a role in damaging the cell membrane.[46] Fig. 4 also shows that the Sample 1 has a similar response against *S. aureus* cells. The antibacterial effect of Sample 1 against *S. aureus* is determined to be ~16%. One possible explanation is that the hydrophilic surface inhibited the *S. aureus* cells from adhering to the surface. Sample 2 did not demonstrate any enhanced antibacterial effect against *S. aureus*. The antibacterial behavior of both Sample 1 and Sample 2 against *S. aureus* cells are found to be similar. One possible explanation for no improvement in antibacterial effect of Sample 2 against *S. aureus* could be that the ZnO structures appear to be agglomerated as evident in the SEM image (Fig. 1(B)). It is also known that Gram-negative bacteria are more susceptible to nanoparticles and nanostructures compared to Gram-positive bacteria. The peptidoglycan layer is 10 times thicker in Gram-positive bacteria compared to the Gram-negative bacteria. The thicker layer of peptidoglycan provides a physical barrier and helps in protecting the bacterial cell. Hence, the rupture of Gram-negative bacteria is easier. It also indicates that the ZnO particles have to sharper to pierce the cell walls of Gram-positive bacteria such as *S. aureus*.
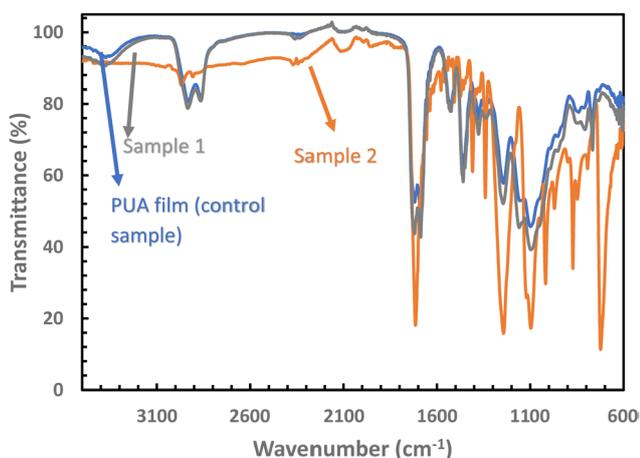

Fig. 3 FTIR spectra recorded for Sample 1 and Sample 2. For comparison, FTIR spectra is also recorded for neat PUA film.
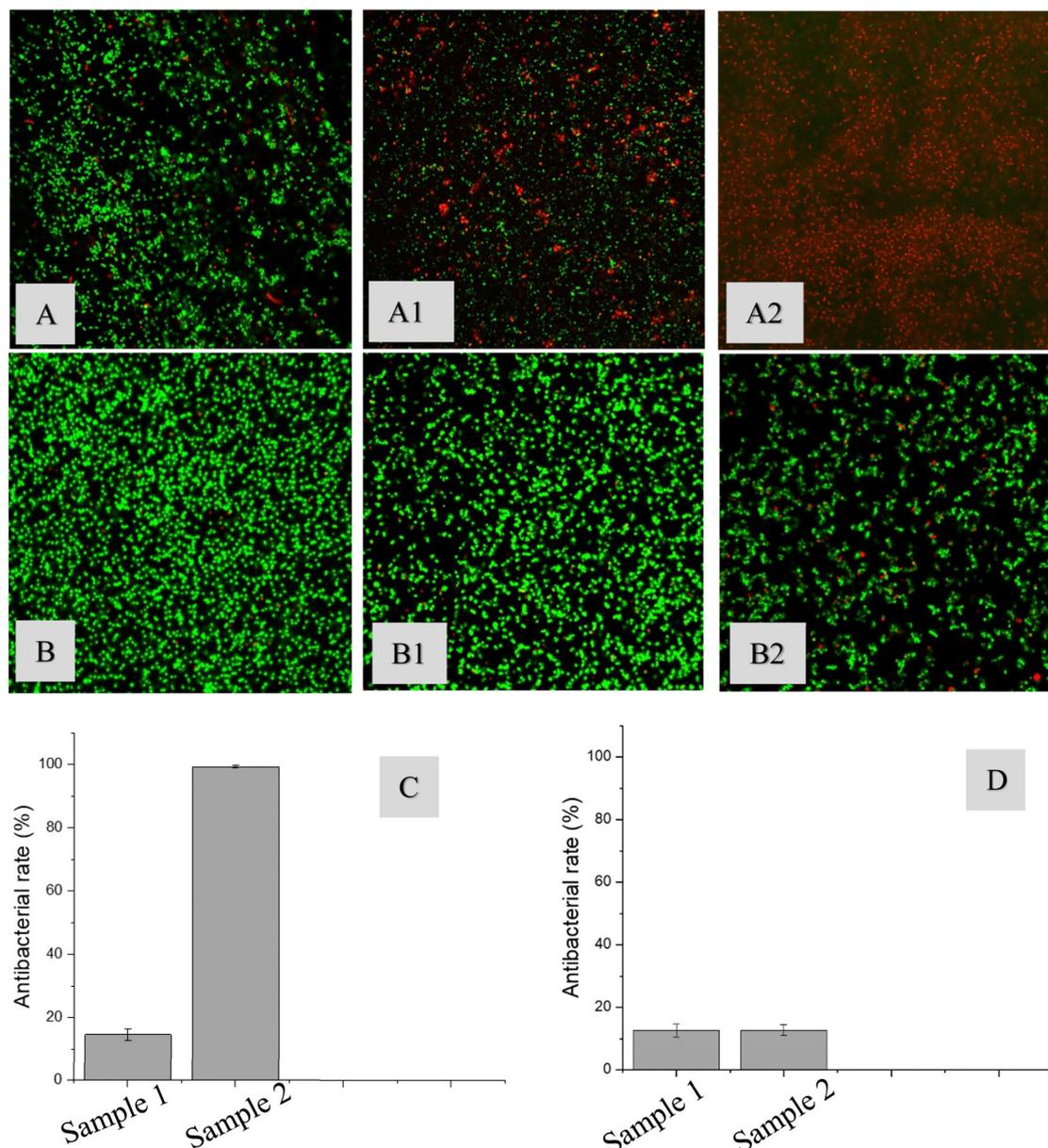
Fig. 4 Confocal microscopy images taken from the surface of the samples to demonstrate their antibacterial behaviour against *P. aeruginosa* and *S. aureus*. The green and red color within these images represent the live and dead bacterial cells respectively. (A) image of control sample with *P. aeruginosa*; (A1) image of Sample 1 with *P. aeruginosa*; (A2) image of Sample 2 with *P. aeruginosa*; (B) image of control sample with *S. aureus*; (B1) image of Sample 1 with *S. aureus*; and (B2) image of Sample 2 with *S. aureus*; (C) antibacterial rate determined for Sample 1 and Sample 2 against *P. aeruginosa*; and (D) antibacterial rate determined for Sample 1 and Sample 2 against *S. aureus*.

This is also supported by the literature, where they argue that the shape of ZnO has a significant effect on its antibacterial behavior against *S. aureus*.[3,28,47] Studies also report that the density of ZnO and the time of interaction between the ZnO and *S. aureus* also determines its antibacterial effect. Sharper and smaller sized ZnO structures are reported to be more toxic as they can easily penetrate the bacterial cell membrane. Babayevska *et al.*[47] also showed that the antibacterial effect of ZnO decreases when its specific surface area is reduced. Thus, *S. aureus* bacterial strain is sensitive to the size, aspect ratio and density of ZnO particles. Our future work will focus on varying

the size and aspect ratio of ZnO structures and investigate its role on its antibacterial effect against *S. aureus*.

4. Conclusion

This study demonstrated the potential of using nanoimprint lithography and a hydrothermal method to produce hierarchical structures on polymer films. In the first step, nanoimprint lithography is used to produce 150 nm diameter pillars on the surface of a PUA film. Following this, a hydrothermal method is

used to grow ZnO nanostructures on the surface of the imprinted PUA film. SEM images demonstrated that the 150 nm diameter pillars are uniformly formed throughout the surface of the PUA film. ZnO structures are formed on the surface of these nanopillars. Following this, the antibacterial behaviour of the sample is investigated against model *P. aeruginosa* and *S. aureus* bacterial cells. The antibacterial results demonstrated that the fabricated sample possesses remarkable efficacy in killing *P. aeruginosa* bacteria. It is effectively in killing ∼100% of the *P. aeruginosa* bacterial cells. This is attributed to the presence of ZnO nanostructures on the surface of the sample. On the other hand, the sample displayed moderate success in killing *S. aureus* bacteria. This is attributed to the shape and size of the ZnO nanostructures formed on the surface of the samples. Further work will be performed to improve the efficacy of these materials. However, the fabriaction technique adopted to produce such hierarchical structures show tremendous promise for use in medical devices and wound dressing materials.

Conflicts of interest

There are no conflicts to declare.

Acknowledgements

References

1 I. Banerjee, R. C. Pangule and R. S. Kane, Antifouling Coatings: Recent Developments in the Design of Surfaces That Prevent Fouling by Proteins, Bacteria, and Marine Organisms, *Adv. Mater.*, 2011, **23**(6), 690–718.

2 J. R. Morones, J. L. Elechiguerra, A. Camacho, K. Holt, J. B. Kouri, J. T. Ramirez and M. J. Yacaman, The Bactericidal Effect of Silver Nanoparticles, *Nanotechnology*, 2005, **16**(10), 2346–2353.

3 A. Sirelkhatim, S. Mahmud, A. Seeni, N. H. M. Kaus, L. C. Ann, S. K. M. Bakhori, H. Hasan and D. Mohamad, Review on Zinc Oxide Nanoparticles: Antibacterial Activity and Toxicity Mechanism, *Nano-Micro Lett.*, 2015, **7**(3), 219–242.

4 V. K. Truong, M. A. Kobaisi, K. Vasilev, D. Cozzolino and J. Chapman, Current Perspectives for Engineering Antimicrobial Nanostructured Materials, *Curr. Opin. Biomed. Eng.*, 2022, **23**, 100399.

5 S. V. Oopath, A. Baji, M. Abtahi, T. Q. Luu, K. Vasilev and V. K. Truong, Nature-Inspired Biomimetic Surfaces for Controlling Bacterial Attachment and Biofilm Development, *Adv. Mater. Interfaces*, 2023, **10**(4), 2201425.

6 S. A. Parekh, R. N. David, K. K. R. Bannuru, L. Krishnaswamy and A. Baji, Electrospun Silver Coated Polyacrylonitrile Membranes for Water Filtration Applications, *Membranes*, 2018, **8**, 59.

7 N. Hoiby, T. Bjarnsholt, M. Givskov, S. Molin and O. Ciofu, Antibiotic Resistance of Bacterial Biofilms, *Int. J. Antimicrob. Agents*, 2010, **35**(4), 322–332.

8 E. R. Kenawy, S. D. Worley and R. Broughton, The Chemistry and Applications of Antimicrobial Polymers: A State-of-the-Art Review, *Biomacromolecules*, 2007, **8**(5), 1359–1384.

9 M. Kong, X. G. Chen, K. Xing and H. J. Park, Antimicrobial Properties of Chitosan and Mode of Action: A State of the Art Review, *Int. J. Food Microbiol.*, 2010, **144**(1), 51–63.

10 A. Jaggessar, H. Shahali, A. Mathew and P. Yarlagadda, Biomimicking Nano and Micro-structured Surface Fabrication for Antibacterial Properties in Medical Implants, *J. Nanobiotechnol.*, 2017, **15**, 64.

11 T. Jiang, M. Deng, R. James, L. S. Nair and C. T. Laurencin, Micro- and Nanofabrication of Chitosan Structures for Regenerative Engineering, *Acta Biomater.*, 2014, **10**(4), 1632–1645.

12 X. Y. Liu, P. K. Chu and C. X. Ding, Surface Nano-Functionalization of Biomaterials, *Mater. Sci. Eng., R*, 2010, **70**(3–6), 275–302.

13 J. Y. Zhu, J. W. Hou, Y. T. Zhang, M. M. Tian, T. He, J. D. Liu and V. Chen, Polymeric Antimicrobial Membranes Enabled by Nanomaterials for Water Treatment, *J. Membr. Sci.*, 2018, **550**, 173–197.

14 G. Vitiello, B. Silvestri and G. Luciani, Learning from Nature: Bioinspired Strategies Towards Antimicrobial Nanostructured Systems, *Curr. Top. Med. Chem.*, 2018, **18**(1), 22–41.

15 C. D. Bandara, S. Singh, I. O. Afara, A. Wolff, T. Tesfamichael, K. Ostrikov and A. Oloyede, Bactericidal Effects of Natural Nanotopography of Dragonfly Wing on Escherichia coli, *ACS Appl. Mater. Interfaces*, 2017, **9**(8), 6746–6760.

16 O. V. Bakina, E. A. Glazkova, A. V. Pervikov and N. V. Svarovskaya, Flower-shaped Micro/nanostructures Based on AlOOH with Antimicrobial Activity Against *E. coli*, *Curr. Nanosci.*, 2019, **15**(5), 525–531.

17 A. Francone, S. Merino, A. Retolaza, J. Ramiro, S. A. Alves, J. V. de Castro, N. M. Neves, A. Arana, J. M. Marimon, C. M. S. Torres and N. Kehagias, Impact of Surface Topography on the Bacterial Attachment to Micro- and Nano-patterned Polymer Films, *Surf. Interfaces*, 2021, **27**, 101494.

18 N. Salah, W. M. Al-Shawafi, A. Alshahrie, N. Baghdadi, Y. M. Soliman and A. Memic, Size Controlled, Antimicrobial ZnO Nanostructures Produced by the Microwave Assisted Route, *Mater. Sci. Eng., C*, 2019, **99**, 1164–1173.

19 A. Baji, V. K. Truong, S. Gangadoo, H. Yin, J. Chapman, M. Abtahi and S. V. Oopath, Durable Antibacterial and Antifungal Hierarchical Silver-Embedded Poly(vinylidene fluoride-*co*-hexafluoropropylene) Fabricated Using Electrospinning, *ACS Appl. Polym. Mater.*, 2021, **3**(8), 4256–4263.

20 E. P. Ivanova, J. Hasan, V. K. Truong, J. Y. Wang, M. Raveggi, C. Fluke and R. J. Crawford, The Influence of Nanoscopically Thin Silver Films on Bacterial Viability and Attachment, *Appl. Microbiol. Biotechnol.*, 2011, **91**(4), 1149–1157.

21 P. Erkoc and F. Ulucan-Karnak, Nanotechnology-Based Antimicrobial and Antiviral Surface Coating Strategies, *Prosthesis*, 2021, **3**(1), 25–52.

22 F. D. Arisoy, K. W. Kolewe, B. Homyak, I. S. Kurtz, J. D. Schiffman and J. J. Watkins, Bioinspired Photocatalytic Shark-Skin Surfaces with Antibacterial and Antifouling Activity via Nanoimprint Lithography, *ACS Appl. Mater. Interfaces*, 2018, **10**(23), 20055–20063.

23 S. M. Dizaj, F. Lotfipour, M. Barzegar-Jalali, M. H. Zarrintan and K. Adibkia, Antimicrobial Activity of the Metals and Metal Oxide Nanoparticles, *Mater. Sci. Eng., C*, 2014, **44**, 278–284.

24 M. Heinlaan, A. Ivask, I. Blinova, H. C. Dubourguier and A. Kahru, Toxicity of Nanosized and Bulk ZnO, CuO and TiO$_2$ to Bacteria Vibrio Fischeri and Crustaceans Daphnia Magna and Thamnocephalus Platyurus, *Chemosphere*, 2008, **71**(7), 1308–1316.

25 Y. N. Slavin, J. Asnis, U. O. Hafeli and H. Bach, Metal Nanoparticles: Understanding the Mechanisms Behind Antibacterial Activity, *J. Nanobiotechnol.*, 2017, 15.

26 T. M. Rashid, U. M. Nayef, M. S. Jabir and F. A. H. Mutlak, Synthesis and Characterization of Au:ZnO (Core:Shell) Nanoparticles via Laser Ablation, *Optik*, 2021, **244**, 167569.

27 K. S. Khashan, F. A. Abdulameer, M. S. Jabir, A. A. Hadi and G. M. Sulaiman, Anticancer Activity and Toxicity of Carbon Nanoparticles Produced by Pulsed Laser Ablation of Graphite in Water, *Adv. Nat. Sci.: Nanosci. Nanotechnol.*, 2020, **11**, 035010.

28 S. V. Gudkov, D. E. Burmistrov, D. A. Serov, M. B. Rebezov, A. A. Semenova and A. B. Lisitsyn, A Mini Review of Antibacterial Properties of ZnO Nanoparticles, *Front. Phys.*, 2021, **9**, 641481.

29 M. Alavi, R. Kowalski, R. Capasso, H. D. M. Coutinho and I. R. A. D. Menezes, Various Novel Strategies for Functionalization of Gold and Silver Nanoparticles to Hinder Drug-Resistant Bacteria and Cancer Cells, *Micro Nano Bio Aspects*, 2022, **1**, 38–48.

30 R. Ahmed, M. Tariq, I. Ali, R. Asghar, P. N. Khanam, R. Augustine and A. Hasan, Novel Electrospun Chitosan/Polyvinyl Alcohol/Zinc Oxide Nanofibrous Mats with Antibacterial and Antioxidant Properties for Diabetic Wound Healing, *Int. J. Biol. Macromol.*, 2018, **120**, 385–393.

31 S. Karagoz, N. B. Kiremitler, G. Sarp, S. Pekdemir, S. Salem, A. G. Goksu, M. S. Onses, I. Sozdutmaz, E. Sahmetlioglu, E. S. Ozkara, A. Ceylan and E. Yilmaz, Antibacterial, Antiviral, and Self-Cleaning Mats with Sensing Capabilities Based on Electrospun Nanofibers Decorated with ZnO Nanorods and Ag Nanoparticles for Protective Clothing Applications, *ACS Appl. Mater. Interfaces*, 2021, **13**(4), 5678–5690.

32 E. A. Munchow, M. T. P. Albuquerque, B. Zero, K. Kamocki, E. Piva, R. L. Gregory and M. C. Bottino, Development and Characterization of Novel ZnO-Loaded Electrospun Membranes for Periodontal Regeneration, *Dent. Mater.*, 2015, **31**(9), 1038–1051.

33 K. Tam, A. Djurišić, C. Chan, Y. Xi, C. Tse, Y. Leung, W. Chan, F. Leung and D. Au, Antibacterial Activity of ZnO Nanorods Prepared by a Hydrothermal Method, *Thin Solid Films*, 2008, **516**(18), 6167–6174.

34 Q. F. Xu, J. N. Wang and K. D. Sanderson, Organic−Inorganic Composite Nanocoatings with Superhydrophobicity, Good Transparency, and Thermal Stability, *ACS Nano*, 2010, **4**(4), 2201–2209.

35 T. J. Athauda, R. R. Ozer and J. M. Chalker, Investigation of Cotton Functionalized with ZnO Nanorods and its Interaction With *E. coli*, *RSC Adv.*, 2013, **3**(27), 10662–10665.

36 D. Q. Pham, S. Gangadoo, C. C. Berndt, J. Chapman, J. L. Zhai, K. Vasilev, V. K. Truong and A. S. M. Ang, Antibacterial Longevity of a Novel Gallium Liquid Metal/Hydroxyapatite Composite Coating Fabricated by Plasma Spray, *ACS Appl. Mater. Interfaces*, 2022, **14**(16), 18974–18988.

37 S. V. Oopath, J. Martins, A. B. Kakarla, I. Kong, A. Petrovski and A. Baji, Rose Petal Mimetic Surfaces With Antibacterial Properties Produced Using Nanoimprint Lithography, *ACS Appl. Bio Mater.*, 2023, **6**, 2690–2697.

38 A. G. Domel, M. Saadat, J. C. Weaver, H. Haj-Hariri, K. Bertoldi and G. V. Lauder, Shark Skin-Inspired Designs That Improve Aerodynamic Performance, *J. R. Soc., Interface*, 2018, **15**, 20170828.

39 A. Elbourne, R. J. Crawford and E. P. Ivanova, Nano-Structured Antimicrobial Surfaces: From Nature to Synthetic Analogues, *J. Colloid Interface Sci.*, 2017, **508**, 603–616.

40 V. K. Truong, R. Lapovok, Y. S. Estrin, S. Rundell, J. Y. Wang, C. J. Fluke, R. J. Crawford and E. R. Ivanova, The Influence of Nano-Scale Surface Roughness on Bacterial Adhesion to Ultrafine-Grained Titanium, *Biomaterials*, 2010, **31**(13), 3674–3683.

41 A. Elbourne, S. Cheeseman, P. Wainer, J. Kim, A. E. Medvedev, K. J. Boyce, C. F. McConville, J. van Embden, R. J. Crawford, J. Chapman, V. K. Truong and E. Della Gaspera, Significant Enhancement of Antimicrobial Activity in Oxygen Deficient Zinc Oxide Nanowires, *ACS Appl. Bio Mater.*, 2020, **3**(5), 2997–3004.

42 J. Hasan, H. K. Webb, V. K. Truong, S. Pogodin, V. A. Baulin, G. S. Watson, J. A. Watson, R. J. Crawford and E. P. Ivanova, Selective Bactericidal Activity of Nanopatterned Superhydrophobic Cicada Psaltoda Claripennis Wing Surfaces, *Appl. Microbiol. Biotechnol.*, 2013, **97**(20), 9257–9262.

43 M. A. Jihad, F. T. M. Noori, M. S. Jabir, S. Albukhaty, F. A. AlMalki and A. A. Alyamani, Polyethylene Glycol Functionalized Graphene Oxide Nanoparticles Loaded with Nigella Sativa Extract: A Smart Antibacterial Therapeutic Drug Delivery System, *Molecules*, 2021, **26**, 3067.

44 H. H. Bahjat, R. A. Ismail, G. M. Sulaiman and M. S. Jabir, Magnetic Field-Assisted Laser Ablation of Titanium Dioxide Nanoparticles in Water for Anti-Bacterial Applications, *J. Inorg. Organomet. Polym. Mater.*, 2021, **31**(9), 3649–3656.

45 A. Valiei, N. Lin, G. McKay, D. Nguyen, C. Moraes, R. J. Hill and N. Tufenkji, Surface Wettability Is a Key

Feature in the Mechano-Bactericidal Activity of Nano-pillars, *ACS Appl. Mater. Interfaces*, 2022, **14**(24), 27564–27574.

46 C. R. Mendes, G. Dilarri, C. F. Forsan, V. D. R. Sapata, P. R. M. Lopes, P. B. de Moraes, R. N. Montagnolli, H. Ferreira and E. D. Bidoia, Antibacterial Action and Target Mechanisms of Zinc Oxide Nanoparticles Against Bacterial Pathogens, *Sci. Rep.*, 2022, **12**, 2658.

47 N. Babayevska, L. Przysiecka, I. Iatsunskyi, G. Nowaczyk, M. Jarek, E. Janiszewska and S. Jurga, ZnO Size and Shape Effect on Antibacterial Activity and Cytotoxicity Profile, *Sci. Rep.*, 2022, **12**, 8148.